Electronic Supplementary Information

Efficient CO_2 electroreduction to CO at low overpotential using a surface-reconstructed and N-coordinated Zn electrocatalyst

Wanan Deng,[a,b,c] Shixiong Min,*[a,b,c] Fang Wang[a,b,c] and Zhengguo Zhang[a,b,c] and Chao Kong[d*]

[a] *School of Chemistry and Chemical Engineering, Key Laboratory of Electrochemical Energy Conversion Technology and Application, North Minzu University, Yinchuan, 750021, P. R. China.*

[b] *Key Laboratory of Chemical Engineering and Technology, State Ethnic Affairs Commission, North Minzu University, Yinchuan, 750021, P. R. China.*

[c] *Ningxia Key Laboratory of Solar Chemical Conversion Technology, North Minzu University, Yinchuan 750021, P. R. China.*

[d] *College of Chemistry and Chemical Engineering, Longdong University, Qingyang, Gansu 745000, P. R. China.*

**Corresponding authors: sxmin@nun.edu.cn; kongchao010@163.com*

1. Experimental

1.1 Preparation of electrodes

A piece of Zn foil (0.5 cm×1.5 cm, thickness: 0.3 mm, 99.99%) was mechanically polished with sandpaper to remove the native oxide layer and then ultrasonic treatment with ethanol, acetone and deionized water sequentially. The newly polished Zn foils were suspended onto the porous SiO_2 griddle of a glass steamer (Fig. S1), which was then transferred into a Teflon-lined autoclave (100 mL), at the bottom of which 5.0 mL of aqueous ammonia solution (25%~28%) was added in advance. Afterward, the Teflon vessel was sealed in the stainless steel autoclave and then transferred to an oven for vapor ammonization treatment at the specified temperatures (90, 120, 150, and 180 °C) and time periods (1, 5, 9 h). Afterward, the obtained ZnO-N samples, was rinsed with deionized water and N_2 blow dried. For a comparison, Zn foil was also treated by the exact same procedures for ZnO-N except that the ammonia solution was replaced by deionized water, and the obtained sample was denoted as ZnO-H. Finally, the thus-obtained ZnO-N and ZnO-H were directly used as the electrodes for electrocatalytic CO_2RR in CO_2-saturated 0.1 M $KHCO_3$ solution, during which the surface oxide was reduced, and the resulted electrodes were denoted as Zn-N and Zn-H, respectively.

1.2 Characterization

X-ray diffraction (XRD) patterns were collected from 5º to 80º in 2θ at a scanning rate of 5º min^{-1} on Rigaku smartlab diffractometer using a nickel filtrated Cu *K*α radiation source at 40 kV and 40 mA. the scanning electron microscopy (SEM) images were obtained on ZEISS EVO 10 for characterizing the prepared samples. Transmission electron microscopy (TEM) and high-resolution TEM (HRTEM) images were taken with a FEI Tecnai-G2-F30 field emission transmission electron microscope. X-ray photoelectron spectroscopy (XPS) analysis was performed on X-ray photoelectron spectrometer (Thermo Scientific Escalab-250Xi) equipped with a monochromatic Al Kα X-ray source.

1.3 Electrochemical measurements

The electrochemical CO_2 reduction experiments were performed with a CHI660E

electrochemical workstation in a two-compartment H-type electrochemical cell. The cathodic and anodic compartments were separated with a Nafion 117 membrane (Nafion 117). An Ag/AgCl (in a saturated KCl solution) and a Pt coil were used as the reference electrode and the counter electrode, respectively, and CO_2-saturated 0.1 M $KHCO_3$ (pH 7.2) was used as electrolyte. All the applied potentials were reported as RHE potentials scale using E (*vs*. RHE)=E (*vs*. Ag/AgCl)+0.656 V–iR_s. The reference electrode was calibrated with a Pt wire as the working electrode for the reversible hydrogen potential in the electrolyte solution purged with N_2 for 30 min and saturated high purity H_2 prior to the measurements. The cyclic voltammetry (CV) was run at a scan rate of 1 mV s^{-1}, and the average of the two potentials at which the current crossed zero was taken to be the thermodynamic potential for the hydrogen electrode reactions.[1] Potentiostatic EIS was used to determine the uncompensated solution resistance (R_s). Liner sweep voltammetry (LSV) measurements for the electrodes was carried out in was performed N_2- or CO_2-saturated 0.1 M $KHCO_3$ solution with a scan rate of 1 mV s^{-1}. For the bulk CO_2 electrolysis, the cathodic compartment was purged with CO_2 (99.999%) at a constant rate of 10 mL min^{-1}. The eluent was delivered directly to the sampling loop of an on-line pre-calibrated gas chromatograph (PANNA GC-A91 plus) equipped with a thermal conductivity detector (TCD) and a flame ionization detector (FID). Faradaic efficiency (FE) of gaseous products at each applied potential was calculated based on following equation:[1]

$$FE_i = \frac{Z_i \times V_i \times G \times t \times p_0 \times F \times 10^{-3}}{Q_{total} \times R \times T_0} \times 100\%$$

where Z_i is number of electrons required to produce an i molecule (CO and H_2; Z_i =2); V_i is volume ratio of product i; G is volumetric flow rate (10 mL·min^{-1}); F is faradaic constant (96485 C mol^{-1}); t is reaction time (min); P_o is atmospheric pressure (101.3 KPa); Q_{total} is integrated charge at each applied potential; R is ideal gas constant (8.314 J·mol^{-1} K^{-1}) and T_o is reaction temperature (298.15 K).

At the end of the electrolysis, the liquid products were analyzed using a high-performance liquid chromatography (HPLC) (HITACHI).

The electrochemical double-layer capacitance of the electrodes was measured in N_2 purged 0.5 M Na_2SO_4 aqueous solution at various scan rates in the scanning potential ranges from -1.18 to -1.08 V (*vs.* Ag/AgCl).[1] The current densities were obtained from the double layer charge/discharge curves at -1.13 V *vs*. Ag/AgCl.

2. Computational method

All calculations were performed by density functional theory (DFT) implemented in Vienna Ab-initio Simulation Package (VASP) with Perdew-Burke-Ernzerhof function (PBE). A plane-wave energy cutoff was fixed at 450 eV and the projector augmented wave method was used for the interaction between ions and electrons. After fully minimizing the bulk structure of Zn with a Monkhorst *k*-point grid of (18×18×18), a (101) Zn surface structure was built by employing vacuum slab of 15 Å as shown in Fig. S11. To avoid discrepancy in surface coverage for each slab model, a (2×4) unit cell were chosen for the (101) surfaces. Additionally, the dipole correction was applied along the z-direction and the top two layers of Zn slabs were only allowed to relax while one bottom layer was fixed to describe the bulk characteristics of Zn crystal. A gamma oriented (4×4×1) k-point grid was employed for Brillouin-zone integrations of the slabs. For the adsorption models, all possible adsorption sites were calculated but the most stable adsorption site was only considered for the free energy calculation. Maximum atomic force of 0.05 eV was chosen as the convergence criterion for structure relaxation. The free energy of adsorbates and non-adsorbed gas-phase molecules is calculated as $G = E_{elec} + E_{ZPE} + \Delta H(0 \to T) + T\Delta S = E_{elec} + G_{(T)}$. The E_{elec} is the reaction energy of the elementary reaction obtained by DFT calculations, E_{ZPE} is the zero point energy estimated under harmonic approximation by taking the vibrational frequencies of adsorbates or molecules as calculated within DFT. The entropies of H_2 (g), CO_2 (g) and CO (g) at 1 atm are used, while the entropy of H_2O (l) is calculated at 0.035 atm, which corresponds to the vapor pressure of liquid water at 298.15 K. Due to the use of PBE functional, the non-adsorbed gas-phase CO molecule has to include a -0.51 eV correction.

3. Addition data

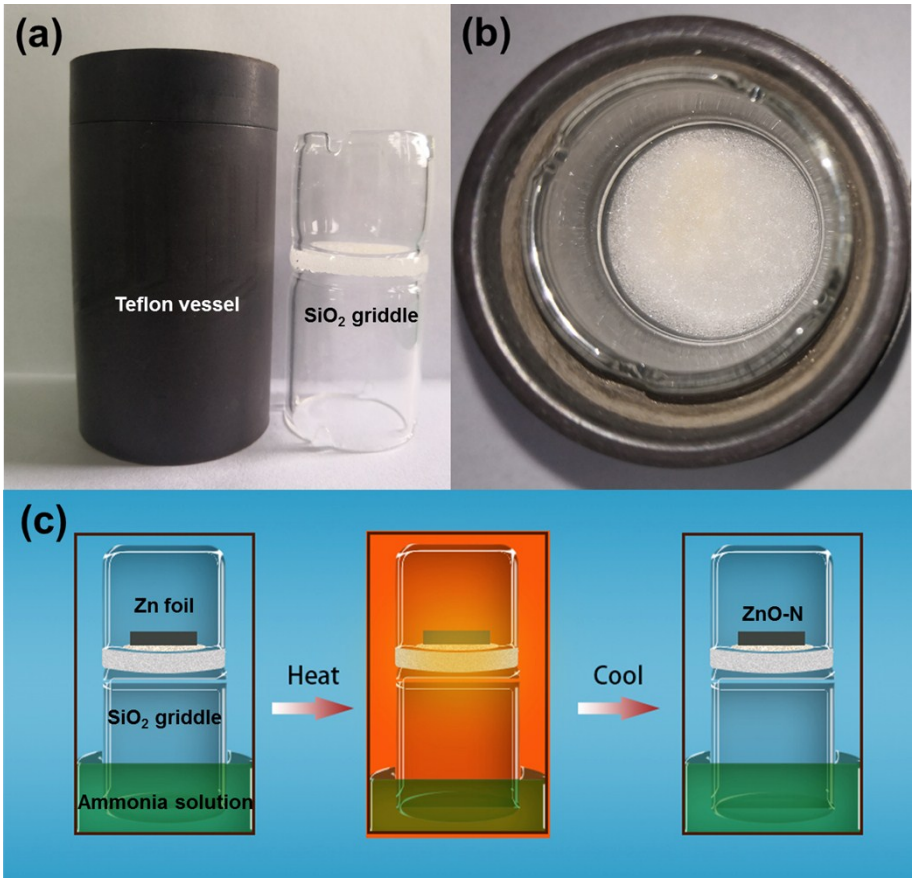

Fig. S1 (a, b) Digital photos of a glass steamer. (c) The schematic procedure of the steaming process for the preparation of ZnO-N.

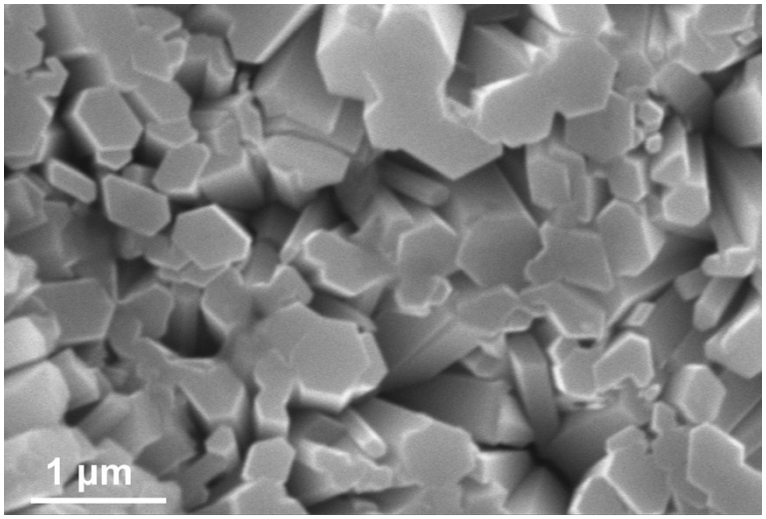

Fig. S2 High-magnification SEM image of ZnO-N.

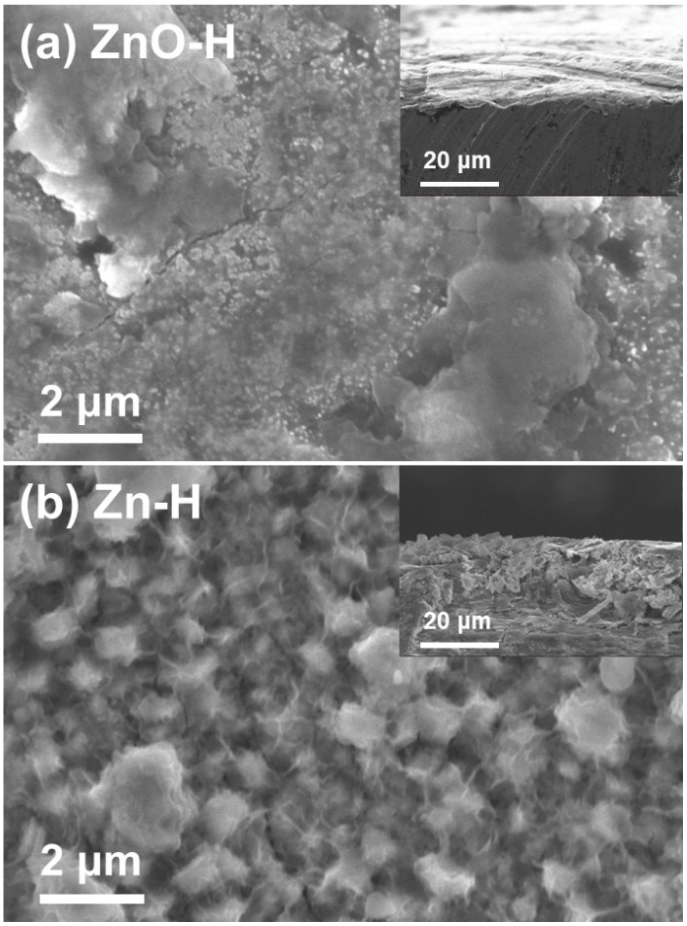

Fig. S3 SEM images of the ZnO-H and Zn-H.

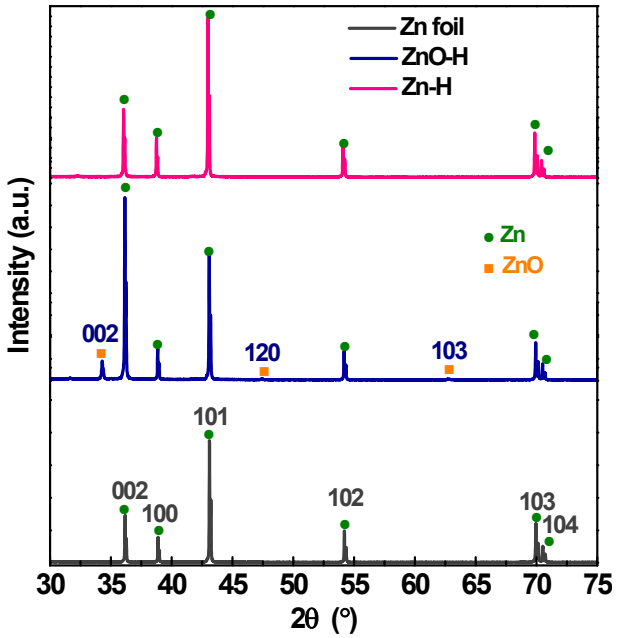

Fig. S4 XRD patterns of the Zn foil, ZnO-H, and Zn-H.

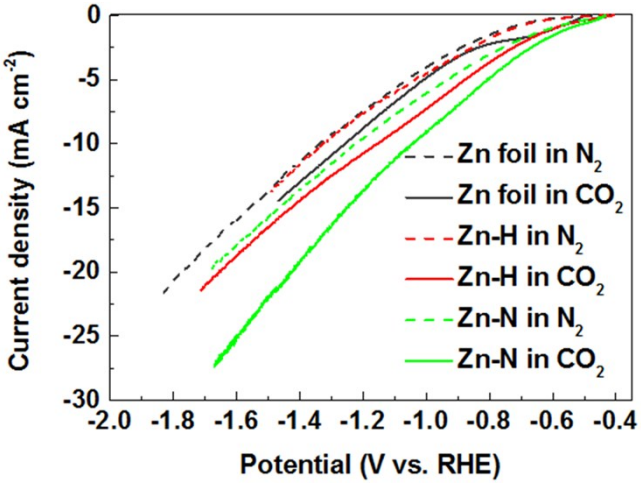

Fig. S5 LSV curves for Zn foil, Zn-H, Zn-N in N_2-and CO_2-saturated 0.1 M $KHCO_3$ electrolyte at a scan rate of 1 mV s^{-1}.

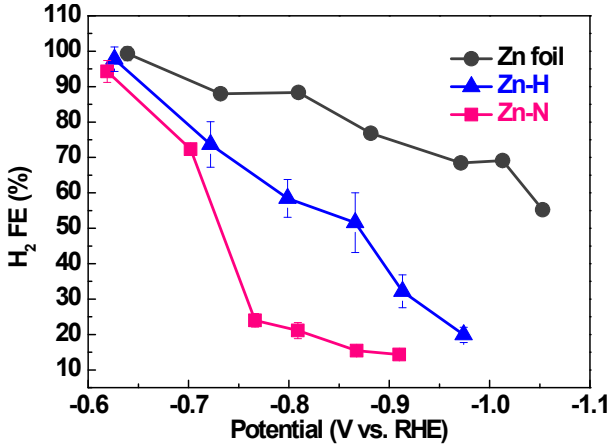

Fig. S6 Potential-dependent H_2 faradaic efficiency for Zn-N, Zn-H, and Zn foil in CO_2-saturated 0.1 M $KHCO_3$ electrolyte.

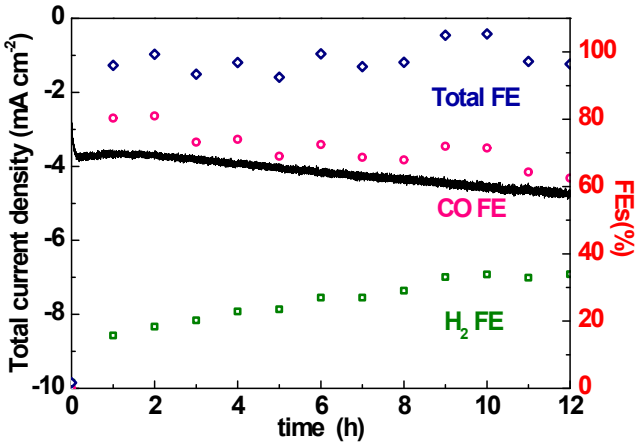

Fig. S7 Electrocatalytic stability of Zn-H electrode for CO_2 reduction in CO_2-saturated 0.1 M $KHCO_3$ at -0.97 V vs. RHE.

Table S1 Comparison of electrocatalytic performances of Zn-based catalysts for CO_2 reduction.

Zn-based catalysts	Electrolyte	Operating potential (V *vs*. RHE)	CO current density (mA cm^{-2})	CO FE	Overpotential for CO_2 reduction (V)	Ref.
Multilayered Zn nanosheets	0.5 M $NaHCO_3$	-1.13	~7.8	86%	1.02	2
Nanowire-like Zn	0.5 M $KHCO_3$	-0.95	~45	98%	0.84	3
Porous-structured-Zn GDE	0.1 M $KHCO_3$	-0.95	~27	94%	0.84	4
Hexagonal Zn	0.5 M $KHCO_3$	-0.95	~28	85.4%	0.84	5
Nanostructured Zn dendrite	0.5 M $NaHCO_3$	-1.1	~16.4	78%	0.99	6
porous network Zn	0.5 M $KHCO_3$	-1.1	~22	88%	0.99	7
Zn/carbon/Ag	0.5 M $KHCO_3$	-1.0	7.3	86%	0.89	8
ZnS/Zn/ZnS	0.1 M $KHCO_3$	-0.8	~9	~94.2%	0.69	9
Oxygen vacancies-rich ZnO nanosheets	0.1 M $KHCO_3$	-1.1	16.1	83%	0.99	10
Ag nanoparticles decorated Zn nanoplates	0.1 M $KHCO_3$	-0.8	~4.9	84%	0.69	11
Nanoscale Zn	0.5 M NaCl	-1.6	~2.2	93%	1.49	12
Porous nanostructured Zn	0.5 M $KHCO_3$	-0.9	6.6	77.8%	0.79	13
Commercial Zn foil	0.1 M $KHCO_3$	-1.3	4.1	78.9	1.19	14
$Zn_{94}Cu_6$ foam	0.5 M $KHCO_3$	-0.95	~11	90%	0.84	15
Porous Zn	0.1M $KHCO_3$	-0.8	~1.2	81%	0.69	16
Zn-N	**0.1 M $KHCO_3$**	**-0.91**	**11.2**	**85.6%**	**0.8**	**This work**

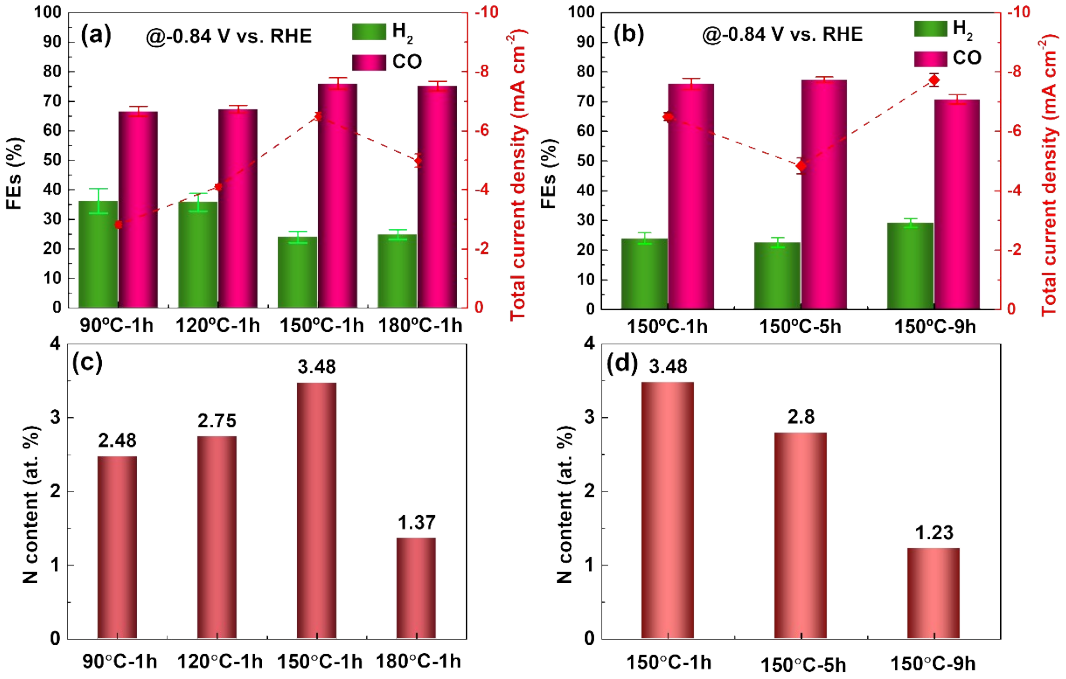

Fig. S8 (a, b) CO_2RR activity of the Zn-N electrodes prepared via the vapor ammonization of Zn foil at specific temperature and time period followed by in situ electroreduction. (c, d) The effects of temperature and time of the vapor ammonization on the N content.

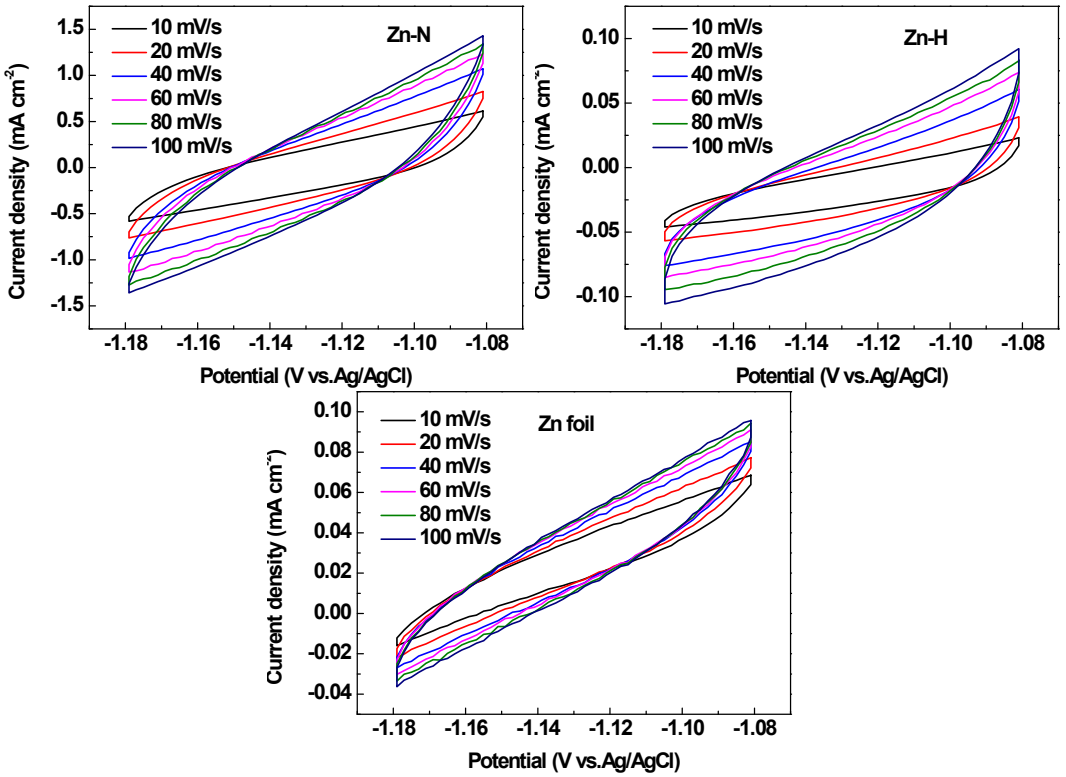

Fig. S9 Cyclic voltammograms (CV) of Zn foil after test, Zn-H and Zn-N at different scan rates.

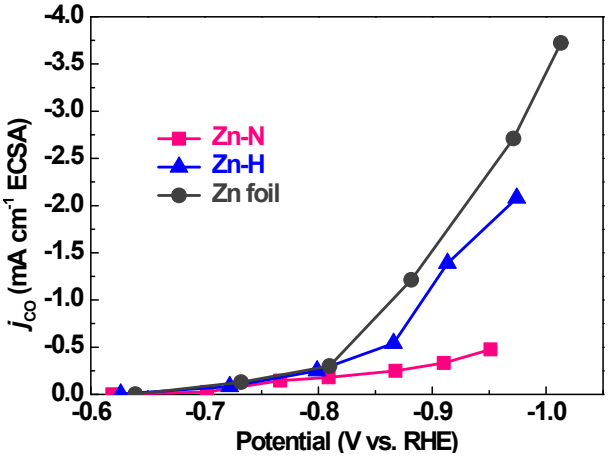

Fig. S10 ECSA-normalized CO current densities for Zn foil, Zn-H, and Zn-N.

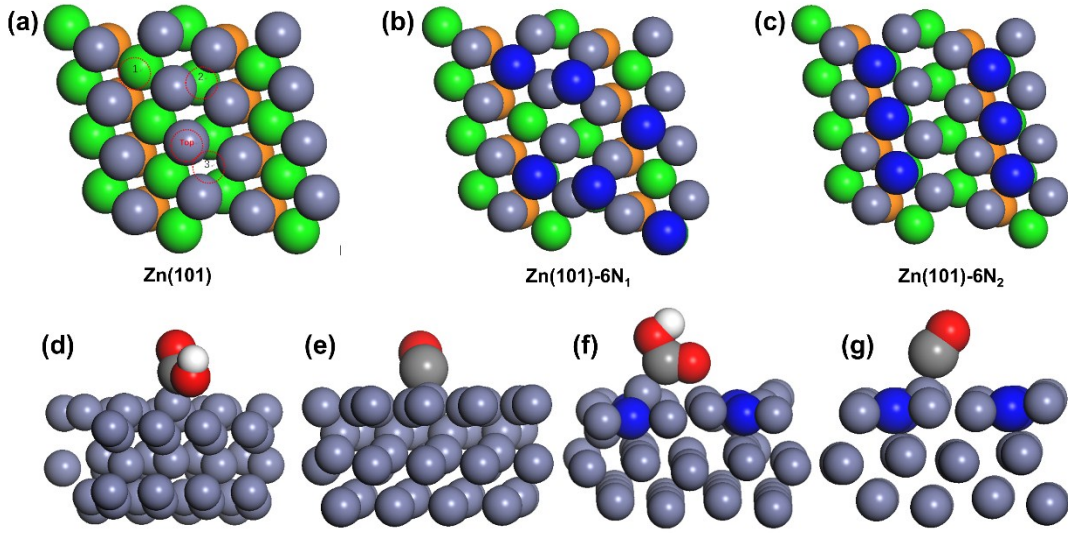

Fig. S11 (a) Zn slab model with (101) facet. (b, c) Atomistic structures constructed for Zn-N electrode according to the results of XPS analysis, and the Zn (101)-6N_2 is identified as the optimal models for Zn-N for DFT calculations. The grey, green, and orange balls represent the Zn atoms at the first, second and third layer, respectively, and the blue balls represent the N atoms. (d) Side-view of *COOH adsorbed on the Zn (101) slab. (e) Side-view of *CO adsorbed on the Zn (101) slab. (f) Side-view of *COOH adsorbed on the Zn (101)-6N_2 slab. (g) Side-view of *CO adsorbed on the Zn (101)-6N_2 slab. The navy blue, gray, red, and white colors represent Zn, C, O, and H atoms, respectively.

Table S2 Zero-point energy corrections and free energy for various system.

System	E (eV)	G_{ZPE} (eV)	G (eV)
Zn-6N_2	-98.98972481	-	-98.98972481
Zn-6N_2-COOH	-126.17842569	0.529169	-125.64925669
Zn-6N_2-CO	-114.09360289	0.098600	-113.99500289
Zn	-51.69195998	-	-51.69195998
Zn-COOH	-78.89626541	0.477469	-78.41879641
Zn-CO	-67.99908183	0.104623	-67.89445883
H_2	-6.75947949	-0.046283	-6.80576249
CO_2	-22.99305859	-0.257516	-23.25057459
H_2O	-14.22483464	-0.001510	-14.22634464
CO	-14.79980944	-0.389399	-15.69920844

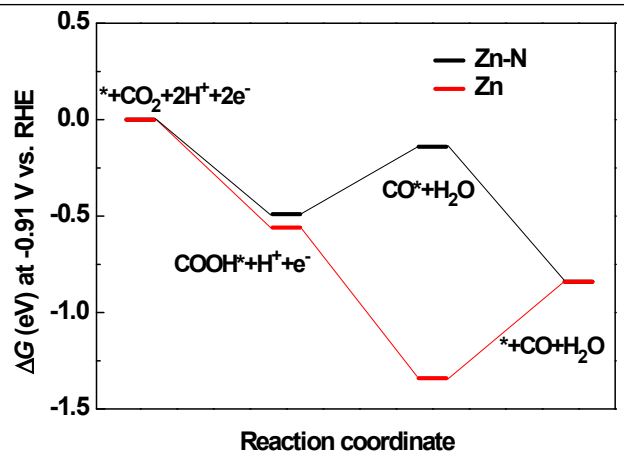

Fig. S12 Free energy diagram at -0.91 V vs. RHE for CO_2 reduction on Zn and Zn-N electrocatalysts.

Reference:

1. S. Min, X. Yang, A.-Y. Lu, C.-C. Tseng, M. N. Hedhili, L.-J Li and K.-W. Huang, *Nano Energy*, 2016, **27**, 121-129.
2. T. Zhang, X. Li, Y. Qiu, P. Su, W. Xu, H. Zhong and H. Zhang, *J. Catal.*, 2018, **357**, 154-162.
3. Y. H. Li, P. F. Liu, C. Li and H. G. Yang, *Chem. Eur. J.*, 2018, **24**, 15486-15490.
4. W. Luo, J. Zhang, M. Li and A. Züttel, *ACS Catal.*, 2019, **9**, 3783-3791.
5. D. H. Won, H. Shin, J. Koh, J. Chung, H. S. Lee, H. Kim and S. I. Woo, *Angew. Chem. Int. Ed.*, 2016, **55**, 9297-9300.
6. J. Rosen, G. S. Hutchings, Q. Lu, R. V. Forest, A. Moore and F. Jiao, *ACS Catal.*, 2015, **8**, 4586-4591.

7. Y. Lu, B. Han, C. Tian, J. Wu, D. Geng and D. Wang, *Electrochem. Commun.*, 2018, **97**, 87-90.
8. F. Yang, P. Song, X. Liu, B. Mei, W. Xing, Z. Jiang, L. Gu and W. Xu, *Angew. Chem. Int. Ed.*, 2018, **57**, 12303-12307.
9. C. Li, G. Shen, R. Zhang, D. Wu, C. Zou, T. Ling, H. Liu, C. Dong and X.-W. Du, *J. Mater. chem. A*, 2019, **7**, 1418-1423.
10. Z. Geng, X. Kong, W. Chen, H. Su, Y. Liu, F. Cai, G. Wang and J. Zeng, *Angew. Chem. Int. Ed.*, 2018, **57**, 6054-6059.
11. Q. Yu, X. Meng, L. Shi, H. Liu and J. Ye, *Chem. Commun.*, 2016, **52**, 14105-14108.
12. F. Quan, D. Zhong, H. Song, F. Jia and L. Zhang, *J. Mater. chem. A*, 2015, **3**, 16409-16413.
13. D. L. T. Nguyen, M. S. Jee, D. H. Won, H. Jung, H.-S. Oh, B. K. Min and Y. J. Hwang, *ACS Sustainable Chem. Eng.*, 2017, **5**, 11377-11386.
14. Z. Chen, K. Mou, S. Yao and L. Liu, *ChemSusChem*, 2018, **11**, 2944-2952.
15. P. Moreno-García, N. Schlegel, A. Zanetti, A. Cedeño López, M. d. J. Gálvez-Vázquez, A. Dutta, M. Rahaman and P. Broekmann, *ACS Appl. Mater. Interfaces*, 2018, **10**, 31355-31365.
16. M. Morimoto, Y. Takatsuji, K. Hirata, T. Fukuma, T. Ohno, T. Sakakura and T. Haruyama, *Electrochim. Acta*, 2018, **290**, 255-261.